Available online at www.sciencedirect.com
SCIENCE DIRECT®
PERGAMON
International Journal of Heat and Mass Transfer 46 (2003) 3765–3775
International Journal of HEAT and MASS TRANSFER
www.elsevier.com/locate/ijhmt

Characterization of the effect of Froude number on surface waves and heat transfer in inclined turbulent open channel water flows

B. Freeze, S. Smolentsev *, N. Morley, M. Abdou

UCLA, Department of Mechanical and Aerospace Engineering, Fusion Science and Technology Center, 44-114 Engineering IV, P.O. Box 951597, Los Angeles, CA 90095-1597, USA

Received 30 December 2002; received in revised form 4 April 2003

Abstract

Interfacial heat transport in open channel turbulent flows is strongly dependent on surface waves that can appear as a result of the interaction of bulk turbulence with the free surface. The paper describes wave/heat transfer phenomena in inclined turbulent open surface water flows. The experiments were conducted in a regime of transition from "weak" to "strong" turbulence, in which the stabilizing influences of gravity and surface tension are relatively small against the disturbing effects of turbulence. A key role of the Froude number, $Fr_{\perp}$, built through the surface-normal component of **g** has been revealed. As $Fr_{\perp}$ grows, the wave amplitude grows, and the frequency spectrum shifts towards shorter waves. These changes lead to a heat transfer improvement, enough to double the heat transfer coefficient. The experimental data have been compared with calculations based on a "K–ε" model. As a result, the range of applicability of the standard model has been established as $Fr_{\perp} < 2000$. The turbulent Prandtl number has been evaluated for $Fr_{\perp} < 700$.

Keywords: Turbulence; Free surface; Heat transfer; Waves; Turbulent Prandtl number

1. Introduction

Open surface turbulent flows with their associated interfacial waves occur widely in nature and are also often used in engineering applications. Heat and mass transport across a flowing liquid interface has become an increasingly important topic during recent research efforts, related to the protection of high heat flux surfaces in fusion reactors [1], as well as many other industrial and ecological processes. A review of the literature revealed numerous mass/heat-transport studies for horizontal, smooth-surfaced subcritical, as well as ocean-type flows (e.g. [2–4]), but less work concerning heat transport for inclined supercritical flows. This tendency is likely due to an interest in turbulent flow analysis in lakes and oceans, to understand the carbon dioxide cycle of the earth [4]. A free surface may be deformed by fluid motion. Such deformations, along with the inherent surface instability, can result in complex wave-type phenomena at the interface. There is a strong correlation between the interfacial waves in the liquid and turbulent scalar transport across the interface. Kutateladze [5] observed the increase in the heat transfer coefficient due to the surface waves by 40–60%. Frisk and Davis [6], and Nakoryakov et al. [7] reported the mass transfer intensification in the carbon dioxide absorption by water of 100–170%. However these observations are mostly related to film flows, in which capillary forces are dominant. In thicker flows, turbulent free surface hydrodynamics as well as heat and mass transfer can vary widely. Moreover, there can be wide differences in the wave behavior at different length

* Corresponding author. Tel.: +1-310-575-9179/794-5366; fax: +1-310-825-2599.
E-mail address: sergey@fusion.ucla.edu (S. Smolentsev).

0017-9310/03/$ - see front matter
doi:10.1016/S0017-9310(03)00197-2

scales, since surface tension is important for short waves and gravity for long waves. Even though the large length scales mostly characterize the flow as a whole, heat or mass transfer depends on the smaller scales [8].

Numerous observations of free surface deformations have shown that key physical mechanisms are related to the stabilization effect of capillary tension and gravity forces against the disrupting effect due to the turbulence kinetic energy (e.g. [9]). Correspondingly, two dimensionless parameters, the Weber number (*We*), and the Froude number (*Fr*) can be introduced, through which the turbulent regimes at the free surface are subdivided into several typical ones. In so-called "weak" turbulence, where both *We* and *Fr* are small (typically $Fr < 1$, $We < 1$), there is little or no surface disturbance. In this regime, once the bulk turbulence reaches the free surface, the turbulent fluctuations become predominantly parallel to the surface. A "blockage" layer with the thickness of the typical turbulence scale is formed in which the normal velocity component is strongly constrained by the free surface, and the scalar transport across the free surface is significantly reduced in comparison with the flow bulk. In contrast to weak turbulence, in "strong" turbulence ($Fr \gg 1$, $We \gg 1$), neither surface tension nor gravity can restrain the fluctuating eddies: the flow breaks up into drops. The absence of a sharp boundary between these two regimes also implies a transition region of marginal breaking that spans a substantial range of *We* and *Fr*, in which different variations between a surface that is no longer smooth and one that is broken can also be observed.

The present study is motivated by the ongoing APEX Project [1], in which a flowing liquid layer of molten salt, such as Flibe or Flinabe, is used for the thermal protection of the fusion reactor first wall. The layer (with a thickness of 2 cm and velocity of 10 m/s) flows along the reactor structural wall and is subjected to a high heat flux (about 2 MW/m^2) from the surrounding plasma. The characteristic features of the flow are a high Froude number ($Fr \sim 10^3$) and high Weber number ($We \sim 10^3$). This implies a reduced effect of capillary forces and gravity on the turbulent interface, in comparison with flows where these two parameters are substantially smaller. The practical question is whether or not the thermal resistance of the turbulent layer in such a flow is low enough to tolerate the heat flux. To study this problem, an experimental loop with a long inclined flume (as a test section with water heated from the side of a free surface) was constructed and simultaneous measurements of the flow thickness and surface temperature were performed using an ultrasound transducer and infrared camera. The goals of the study were twofold. First, the experimental data for the flow thickness were statistically analyzed to characterize the surface waves. Second, the heat transfer measurements were analyzed together with calculations conducted with a K–ε model of turbulence to evaluate the turbulent Prandtl number in the wavy flows. Additionally, a conclusion on the applicability of the K–ε model to the wavy flows was drawn by comparison of the experimental and calculated data for the mean flow thickness.

2. Experiment

The experiments were conducted using a water loop (Fig. 1) since the physical properties of the molten salts of interest do not substantially differ from those of water. The test section is a 4-m long, 40-cm wide inclined flume. The working fluid is injected continuously into the test section by two centrifugal pumps (up to 75 l/s), connected in parallel through an adjustable nozzle (3–50 mm height). The nozzle has a honeycomb and a secondary screen to reduce the inlet turbulence. The nozzle height is adjusted to provide an inlet flow thickness closer to the equilibrium one. This reduces the transition length significantly. The liquid is collected into a 1-m^3 tank at the bottom of the supporting frame. An infrared (IR) heater (30 cm × 30 cm, up to 60 kW/m^2) located 3 m down from the nozzle is used to heat the liquid from the side of the free surface. All measurements are conducted immediately after the heated area, where the mean flow is hydrodynamically fully developed. The measurements include IR images from the FLIR-600 IR camera, as well as the flow thickness versus time measured by the 10 MHz 3 mm V129-RM Panametrics ultrasound transducer. A more detailed description of the experimental facilities and approaches is given in [10].

In the experiments, the flow rate, the inclination angle, and the nozzle height can be changed to provide a wide range of dimensionless flow parameters. The basic dimensional and dimensionless parameters are listed in Table 1. In the table, α is the flume inclination angle with

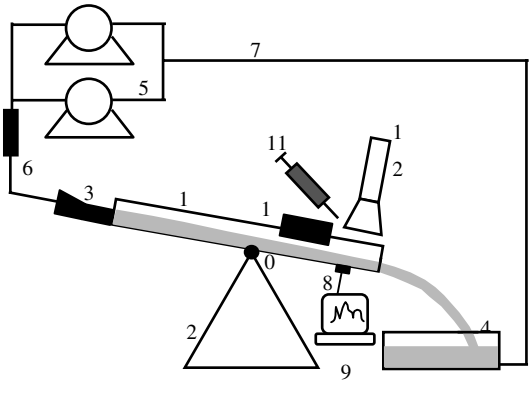

Fig. 1. Schematic of experimental equipment: 1. inclined test-section, 2. frame, 3. nozzle, 4. tank, 5. two pumps, 6. flowmeter, 7. hoses, 8. ultrasound transducer, 9. PC, 10. IR heater, 11. dye injector, 12. IR camera.

Table 1
Experimental parameters

α (deg)	U_m (m/s)	h_m (m)	Re	Fr	$Fr_\perp$	We	$h_{K-\varepsilon}$ (m)	δ %	σ (m)	σ/h_m
0.1	0.452	0.0221	10,000	0.94	0.94	60	0.0232	4.9	0.0004	1.8
3.5	1.45	0.0100	14,500	25	25	280	0.0097	3.0	0.0007	7.0
3.5	2.03	0.0120	24,250	50	50	670	0.0126	5.0	0.0009	7.5
30	2.91	0.0044	12,750	190	220	500	0.0046	4.5	0.0009	20.5
30	3.90	0.0068	26,500	230	260	1400	0.0070	3.0	0.0012	17.7
30	4.57	0.0081	37,000	260	300	2280	0.0086	6.2	0.0014	17.3
50	3.71	0.0060	26,000	320	500	1120	0.0060	0.0	0.0013	21.7
50	5.40	0.0070	37,750	430	670	2760	0.0075	7.1	0.0015	21.4
50	6.01	0.0084	50,500	440	680	4100	0.0090	7.1	0.0021	23.3
75	5.10	0.0051	26,000	520	2010	1790	0.0056	9.8	0.0012	23.5
75	6.47	0.0058	37,500	720	2790	3280	0.0069	19.0	0.0016	27.6
75	7.94	0.0063	50,000	1250	4830	5230	0.0083	31.7	0.0022	34.9

respect to the horizontal; U_m and h_m are the bulk velocity and mean flow thickness in the reference cross-section. $Re = U_m h_m/\nu$, $Fr = U_m^2/gh_m$, and $We = U_m^2\rho h_m/\sigma_T$ are the bulk Reynolds, Froude, and Weber number, respectively. An alternative definition of the Froude number, $Fr_\perp = Fr/\cos\alpha$, which is built through the component of **g** normal to the flume bottom, is also shown. In theoretical considerations, sometimes it is more appropriate to define $Fr_\perp$ through the component of **g** normal to the mean air–water interface. However, in most of the experiments, the measurements were conducted within the fully developed flow section, over which both definitions of $Fr_\perp$ result in the same numbers. The variable $h_{K-\varepsilon}$ is the mean flow thickness calculated with the K–ε model, σ is the standard deviation of the flow thickness, and $\delta = (h_{K-\varepsilon} - h_m)/h_m$. The first row in the table corresponds to a hydraulically subcritical flow, which was realized to test the present approach against the previous data by Ueda et al. [2]. The rest of the experimental points stand for a supercritical flow. A number of measurements at $\alpha = 30°$ for a supercritical flow had been conducted before using the same facilities [11]. These data are not shown in the table, but were used in the present analysis along with the current ones.

The speed of the liquid in almost all of the experiments is not too high and the surrounding air is stagnant, such that only a low shear rate can be produced at the free interface. Thus, the flow conditions that correspond to no waves being generated by the wind were established. The experimental facility does not have special tools to completely eliminate the air entrainment effect. However, photographs of the flow, as well as visual observations, have not revealed any air bubbles entrained in the water.

3. "*L–q*" diagram

A convenient way of approximate characterization of the free surface regime in comparison with the other possible open channel flows is the "*L–q*" diagram (Fig. 2), recently suggested in [9]. Rather than using the Weber and Froude numbers, this diagram operates with two dimensional parameters, L and q, which are the length scale and the overall velocity of a typical turbulent element of fluid near the free surface. In the diagram, the (L, q)-plane is subdivided into four regions by the two dotted lines, which are simply defined by critical values of We and Fr. In addition to the already mentioned weak and strong turbulence regions, the diagram shows two others with no surface disintegration, in which gravity or surface tension is a major factor, and the surface phenomena associated with gravity or capillary waves are correspondingly dominant. The area

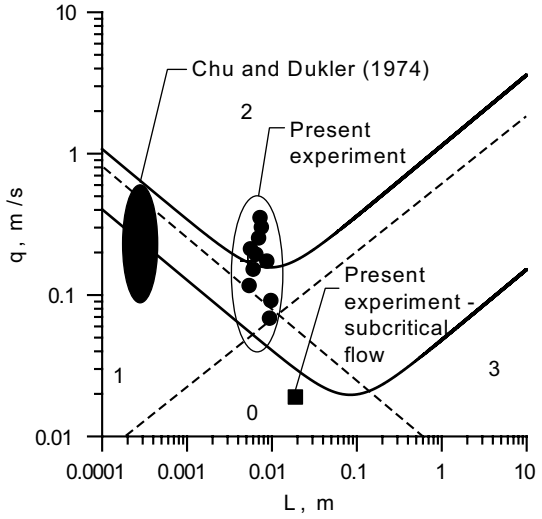

Fig. 2. *L–q* diagram for water adapted from [9] with the present experimental data and data for film flows. Region 0 is weak turbulence. Region 2 is strong turbulence. Region 1 is turbulence with surface tension dominant over gravity. Region 3 is gravity-dominated turbulence. The area between the two solid lines represents transitional region of marginal breaking.

between the two solid lines represents the transitional region of marginal breaking. The boundaries of the transitional region are calculated with simplified models for the idealized spherical turbulent blobs. The present experimental data are plotted in the diagram with the friction velocity as q, and the flow thickness as L. Using the flow thickness as a scale for the turbulent structures is reasonable as an estimation, because in channel flows the characteristic size of the turbulent vortices generated in the flow is controlled by the characteristic channel cross-sectional dimension. The present data run mostly into the transitional regime, with about equal effect of gravity and surface tension. This is in a qualitative agreement with the experimental observations of the free surface; large-amplitude waves and almost no splashing have been observed. Some insignificant drop formation was noticed at $\alpha = 75°$. Visual observations showed much more waviness at the surface as the flow rate and/or the inclination angle grew. Directly at the nozzle, the free surface is smooth; the surface waves grow in amplitude downstream reaching a quasi-saturation state over some distance (1–2 m) from the nozzle, which varies depending on the flow parameters.

Unlike the present experiments, typical film flow data, for example those in the experiments by Dukler et al. [12–14] for thin vertically moving water films, run into the region of turbulence with surface tension dominant over gravity. More detailed comparisons in the next section show sufficient discrepancy in the wave behavior between these two data sets.

4. Statistical characteristics of the free surface

Although the "L–q" diagram is an effective approach to give a qualitative description of surface turbulence, it is not enough itself to fully characterize the phenomena. Detailed considerations are needed through a statistical analysis of the experimental data. In the present study, the fluctuating flow thickness was measured as a function of time at a given point within the fully developed flow section employing an ultrasound transducer. The statistical analysis performed on the experimental data is similar to that developed by Dukler et al. [12–14] for film flows. It included evaluation of the mean flow thickness and its standard deviation, probability density function, and power spectral density.

Each of the $h(t)$ curves (Fig. 3) is based on the subsequent measurements of the flow thickness taken with a time increment of one millisecond. The number of the measurements in one sample is limited by the hardware capabilities and usually consisted of 509 data points. The water–air interface demonstrates irregular wave-type behavior with wave frequency and amplitude increasing with inclination angle. The probability density function of $h(t)$ is very well approximated with the Gaussian fit (Fig. 4). Similar distributions were observed in horizontal open-surface flows of about 2.5 cm thick [15], which fall into the same area in the "L–q" diagram as most of the present data. At the same time, the experiments with the vertically moving water films thinner than 1 mm [12–14] showed a so-called "two-wave system" [12] appearing in the form of large lumps of liquid and smaller waves imposed on these large structures. However, both the large and smaller structures had wavelengths shorter than 1.74 cm and hence were capillary waves. Such waves are better described by the gamma rather than Gaussian distribution [12]. In all of the present experiments, no discrepancies from the Gaussian fit were noticed. Thus, it is most likely that the formation of the two-wave system is not related to the flow regimes considered in the present experiments.

To estimate the power spectral density (PSD), Welch's averaged periodogram method was applied [16]. However, applying this method to a single 509-point data sample does not result in a well-behaved curve

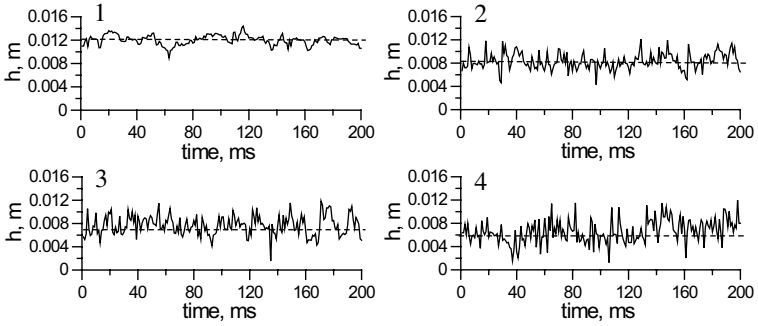

Fig. 3. Flow thickness vs. time measured with the ultrasound transducer. 1: $\alpha = 3.5°$, $Re = 24{,}250$, $Fr_{\perp} = 50$, $h_m = 0.012$ m, $\sigma = 0.0009$ m. 2: $\alpha = 30°$, $Re = 37{,}000$, $Fr_{\perp} = 260$, $h_m = 0.008$ m, $\sigma = 0.0014$ m. 3: $\alpha = 50°$, $Re = 37{,}750$, $Fr_{\perp} = 670$, $h_m = 0.007$ m, $\sigma = 0.0015$ m. 4: $\alpha = 75°$, $Re = 37{,}500$, $Fr_{\perp} = 2790$, $h_m = 0.0058$ m, $\sigma = 0.0016$ m.

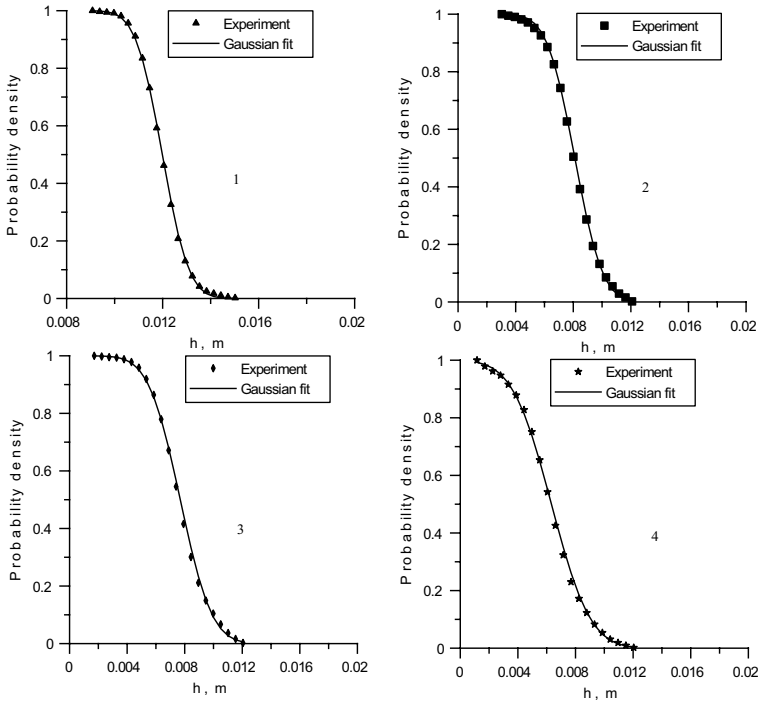

Fig. 4. Probability density of $h(t)$. Experiment vs. Gaussian fit. 1: $\alpha = 3.5°$, $Re = 24{,}250$, $Fr_\perp = 50$, $h_m = 0.012$ m, $\sigma = 0.0009$ m. 2: $\alpha = 30°$, $Re = 37{,}000$, $Fr_\perp = 260$, $h_m = 0.008$ m, $\sigma = 0.0014$ m. 3: $\alpha = 50°$, $Re = 37{,}750$, $Fr_\perp = 670$, $h_m = 0.007$ m, $\sigma = 0.0015$ m. 4: $\alpha = 75°$, $Re = 37{,}500$, $Fr_\perp = 2790$, $h_m = 0.0058$ m, $\sigma = 0.0016$ m.

because of the spectral noise. To reduce the spectral noise, many more data sets were used. The resulting frequency spectra were then averaged to form a single frequency spectrum in which the spectrum noise was reduced in proportion to the square root of the number of samples, to a level allowing interesting features to be resolved (Fig. 5).

These obtained PSDs demonstrate a large peak at about 10–40 Hz, as well as a long "tail" of higher frequency modes. Although the wave celerity has not been evaluated in the experiment, simple estimations based on the PSD data and the mean flow speed show that the wavelengths range from several millimeters to tens of centimeters. Therefore, both capillary and gravity waves are presented in the spectrum. As the inclination angle (or $Fr_\perp$) grows, the contribution of shorter waves becomes more significant, making the interface more irregular. This tendency towards a more uniform spectrum is summarized in Fig. 6, where the PSD maximum and minimum are plotted versus $Fr_\perp$.

The effect of the flow speed and inclination on the wave amplitude is illustrated in Fig. 7, where a waviness parameter is plotted as a function of Re and α. The figure also elucidates the range of applicability of the K–ε model (for detailed explanations see the next section). The waviness parameter is defined here as the ratio of the standard deviation of the flow thickness to the mean thickness, σ/h_m. Since this parameter is within 0.01–0.35, the waves observed should be classified as finite-amplitude waves. One can see that the waviness is mostly dependent on the inclination angle and to a smaller degree on Re. For example, at $\alpha = 30°$, the waviness parameter slightly decreases even though the Reynolds number varies in a wide range. However, at deep inclinations closer to vertical flow, the effect of the velocity becomes more pronounced, and an increase in velocity results in a sufficiently higher σ/h_m ratio. In Fig. 8, the same data as in Fig. 7 are plotted as a function of $Fr_\perp$ using a semi-log scale. One can see that the effect of the velocity and the inclination angle on the wave amplitude is described very well using $Fr_\perp$ only. The best fit, which relates the waviness parameter to $Fr_\perp$, was found to be

$$\sigma/h_m = 5.11 \times 10^{-03}(\ln Fr_\perp)^2 - 2.60 \times 10^{-03} \ln Fr_\perp + 0.015. \quad (1)$$

It is clear that reducing the stabilizing action of gravity against the disturbing influence of turbulence at higher $Fr_\perp$ causes the observed effects of this parameter on both the wave amplitude and frequency. At deeper inclinations, more and more turbulent elements from the flow bulk (smaller in size) can deform the free surface, resulting in more irregular interface behavior.

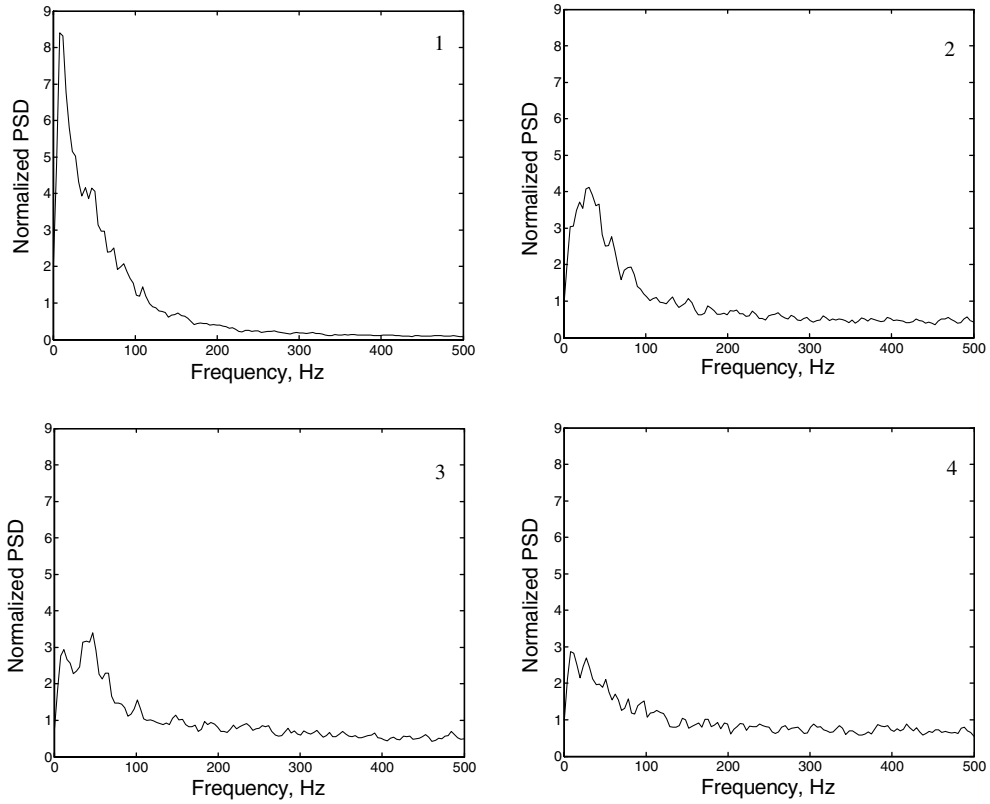

Fig. 5. Typical spectra of $h(t)$ based on averaging 50 data samples, 509 data points each. 1: $\alpha = 3.5°$, $Re = 24{,}250$, $Fr_\perp = 50$. 2: $\alpha = 30°$, $Re = 37{,}000$, $Fr_\perp = 260$. 3: $\alpha = 50°$, $Re = 37{,}750$, $Fr_\perp = 670$. 4: $\alpha = 75°$, $Re = 37{,}500$, $Fr_\perp = 2790$.

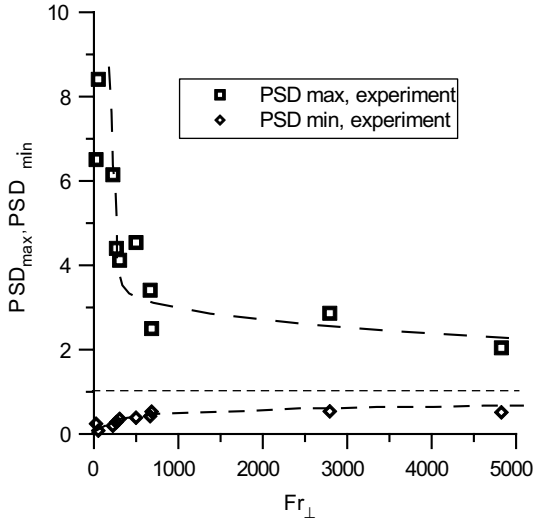

Fig. 6. PSD maximum and minimum vs. $Fr_\perp$.

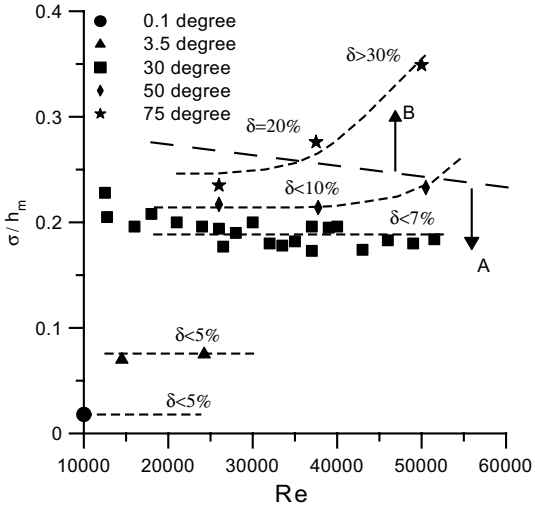

Fig. 7. The effect of the flow speed and inclination on the wave amplitude. The dashed line subdivides the plot area into two zones, A and B. In A, the K–ε predictions of the mean flow thickness are within the 10% accuracy of the experimental data.

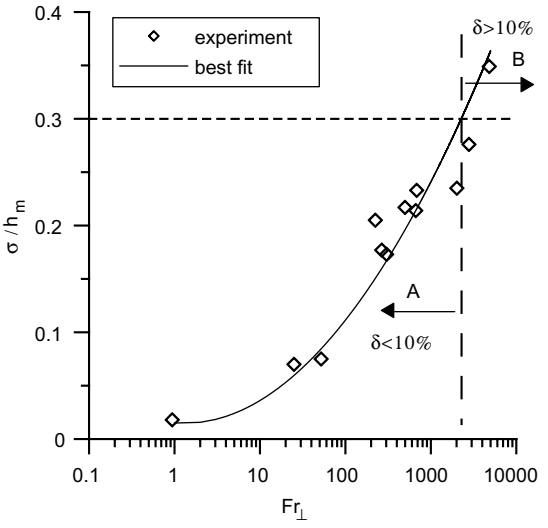

Fig. 8. The waviness parameter as a function of $Fr_{\perp}$. If σ/h_m is smaller than about 0.3 (area A), the K–ε predictions of the mean flow thickness are accurate enough. At higher waviness (area B), the K–ε predictions are unsatisfactory.

5. Application of the K–ε model to calculations of the mean flow thickness

The present experimental data were used to clarify the limitations of the K–ε model when applied to calculations of turbulent open channel flow with surface waves. A particular variant of the low-Reynolds number model in the form proposed by Chien [17] with the free surface boundary conditions analogous to those by Hossain and Rodi [18] have been chosen based on the previous authors experience [19]. This model is referred here as a "standard" two-equation model for open channel flows. The mean equations being solved are written in the Cartesian coordinates using the thin-shear-layer approximation with the x-axis in the main flow direction, the y-axis perpendicular to the flume bottom, and the coordinate origin located on the bottom in the inlet cross-section, as follows:

$$\frac{\partial U}{\partial t}+U\frac{\partial U}{\partial x}+V\frac{\partial U}{\partial y}=-g\cos(\alpha)\frac{\partial h}{\partial x}+g\sin(\alpha)+\frac{\partial}{\partial y}\left[(\nu+\nu_{\mathrm{t}})\frac{\partial U}{\partial y}\right], \tag{2}$$

$$\frac{\partial U}{\partial x}+\frac{\partial V}{\partial y}=0, \tag{3}$$

$$\frac{\partial h}{\partial t}+U_s\frac{\partial h}{\partial x}=V_s. \tag{4}$$

Here, $U(t,x,y)$ and $V(t,x,y)$ are the mean velocity components, $h(t,x)$ is the mean flow thickness, and ν and ν_{t} are the kinematic and turbulent viscosity. The subscript "s" denotes the free surface. The turbulent viscosity is constituted by the Kolmogorov–Prandtl expression: $\nu_{\mathrm{t}}\sim K^2/\varepsilon$, with the turbulent kinetic energy, K, and its dissipation rate, ε, governed by the aforementioned K–ε equations. Eqs. (2) and (3) are used to calculate the mean velocity. Eq. (4), the kinematic free surface condition, is used to calculate $h(t,x)$. The boundary conditions consist of a no-slip condition at the solid wall and no-tangential stress at the free surface.

The equations were approximated with the finite-difference formulas using a stretched grid, which concentrates grid points near the bottom wall and the free surface. To provide for proper resolution in the wall vicinity, the number of grids across the flow was varied between 50 and 200, depending on the turbulence Reynolds number, with the first grid point located between $y_+=0.1$ and $y_+=0.5$. The solution was sought as the steady-state solution of a time-dependent problem, using a Blottner-type finite-difference method [20] with a surface-height method as a technique for tracking the free surface [21]. Validations of the model (by comparing it to experimental data) for flows with no waves were performed in the previously cited paper [19].

In accordance with [22] the turbulent structure of open channel flows can be subdivided into three characteristic sub-regions: the wall region ($y/h<0.15$–0.2), the intermediate region (0.15–$0.2<y/h<0.6$), and the free surface region ($0.6<y/h<1.0$). If there are no waves, the first two sub-regions are not strongly influenced by the free surface and behave like the viscous sub-layer and log-layer in near-wall turbulent flows, respectively. The standard model describes this situation very well. However, once the waviness becomes high, the turbulence structure is different. One can expect a large amount of bulk turbulence-free surface interaction, a mechanism that is not included in the standard model.

The comparison of the mean flow thickness calculated with the standard K–ε model with that from the present experiment gives a range of applicability of the model. If the waviness is relatively small, the coincidence is good enough (Fig. 9). However, the discrepancy grows with the waviness parameter (Table 1, and Figs. 7 and 8). In high waviness regimes, the K–ε model always overestimates the mean flow thickness. At high σ/h_m, the model gives inaccurate predictions. The area of applicability of the model is shown in Fig. 8, where a level of 10% difference exists with the experimental data, taken as a conventional boundary. The critical value of the waviness parameter was found to be 0.3. In accordance with formula (1), it corresponds to $Fr_{\perp}\approx 2000$. This is also the level of waviness where the free surface disturbances can extend all the way down to the bottom wall of the flow.

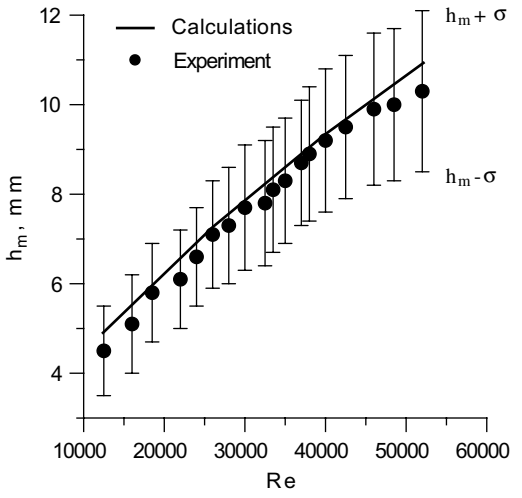

Fig. 9. Comparison of the calculated mean flow thickness with the experimental data at $\alpha = 30°$. The waviness parameter is about 0.2.

6. Heat transfer and evaluation of Pr_t

In the context of the present study, the heat transfer problem can be described by the mean energy equation

$$\rho C_p\left(\frac{\partial T}{\partial t} + U\frac{\partial T}{\partial x} + V\frac{\partial T}{\partial y}\right) = \frac{\partial}{\partial y}\left(k_{\text{eff}}\frac{\partial T}{\partial y}\right) \tag{5}$$

and the boundary condition at the free surface that simulates a heat flux, q, applied to the surface within the heated area. Here k_{eff} is the effective thermal conductivity coefficient that stands for both the molecular and turbulent heat transport, $k_{\text{eff}} = k + k_t$, $T(t,x,y)$ is the temperature in the liquid, and ρ and C_p are the fluid mass density and specific heat. Eq. (5) utilizes the commonly accepted model for the mean turbulent heat flux given by the extension of the Fourier law for the heat conduction as follows:

$$\langle t'v'\rangle = -\frac{v_t}{Pr_t}\frac{\partial T}{\partial y},$$

so that

$$k_t/k = \frac{v_t}{v}\frac{Pr}{Pr_t}.$$

The turbulent Prandtl number in this formula, Pr_t, is the ratio of the eddy diffusivity for momentum to the eddy diffusivity for heat. To describe properly the heat transport in the free surface region, Pr_t should be evaluated from experimental data. Previous evaluations were performed for subcritical water flows [19], in which Pr_t was calculated by using the eddy diffusivity for momentum obtained with the K–ε model and eddy diffusivity for heat taken from the experimental data [2]. The best fit was found as

$$Pr_t = 0.7 \times [1 + \exp\{A \times (y/h_m - 0.89)\}],$$
$$A = 37.0 \text{ (subcritical flow)}. \tag{6}$$

This shows an essential anisotropy in the near-surface turbulence and, as a result, significant heat transfer degradation within the blockage layer. The present evaluations for high Fr, high We flows also adopt Eq. (6), but unlike the direct approach in [19] are based on an indirect method that adjusts the parameter A through matching the experimentally measured surface temperatures with those calculated by using Eq. (5). When solving Eq. (5), the velocity distribution and the turbulent viscosity profile used as input data to a heat transfer code were calculated with the standard K–ε model and the flow equations (2)–(4) presented in Section 5. The heat transfer code implements the same finite-difference formulation as described in Section 5.

A typical thermal image of the free surface, right after the flow exits the lower heater edge region, taken with the IR camera, is shown in Fig. 10. The temperature field of the free surface is essentially non-uniform and time varying. One can see "hotter" and "cooler" spots in the form of streaks elongated in the flow direction, that appear due to the significant interface irregularities. The temperature non-uniformity seen in the image can serve as an indirect confirmation of the overturning waves and surface renewal phenomena. Some extra information could be obtained by evaluating the spectra for the oscillating temperature field and then comparing them with those for the oscillating flow thickness. However these spectra were not obtained since the IR camera did not provide high enough resolution in time. To obtain the mean temperature distribution along the main flow direction, the thermal images were averaged in the spanwise direction over the 20 cm strip and in time, for a period of approximately 10 s. If

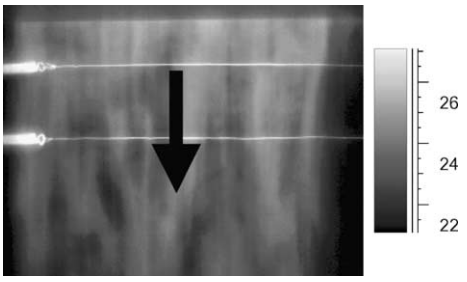

Fig. 10. Typical snapshot of the water surface with the IR camera. The arrow shows the flow direction. The heat flux is applied to the free surface. Two thin strips in the spanwise direction are the thermal images of heated wires located above the surface, which are used as a length scale. The wires are 5 cm apart.

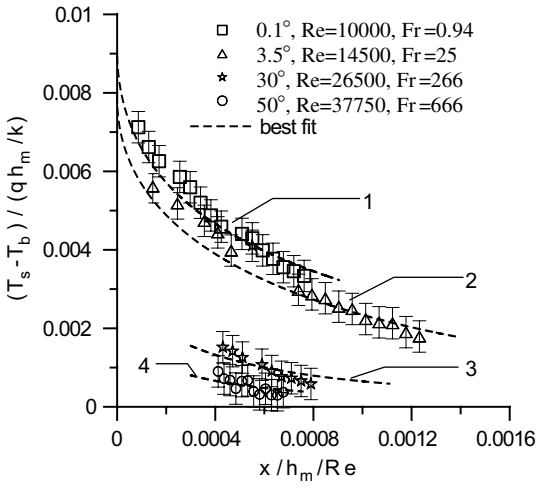

Fig. 11. Dimensionless mean surface temperature profiles measured in the experiment and calculated. The calculations of the temperature were performed using Eqs. (2)–(4), the K–ε equations from [19], and the energy equation (5). The parameter A in formula (6) for Pr_t has been evaluated as follows. 1: $A = 37.9$; 2: $A = 35.3$; 3: $A = 29.0$; 4: $A = 27.1$.

these data are plotted in a dimensional form in the same figure, the experimental points are mixed making their comparison difficult. To present the data in a comparable form, it is reasonable to introduce scales, such as qh_m/k as a temperature scale and h_m/Re as a length scale. The choice of the scales is based on the dimensionless form of the energy equation (5). Such dimensionless temperature profiles after averaging are shown in Fig. 11. Once the liquid leaves the heated area, the mean surface temperature drops fast due to transport of heat into the flow bulk. The separation of temperature curves in the figure is explained by increasing the cooling rate in the free surface vicinity as the waviness grows. In terms of the K–ε model adopted in the present study, increasing the coolant rate means lower values of Pr_t. The improvement of heat transfer is directly related to better mixing of liquid at the free surface due to relatively short waves with the characteristic dimension comparable with the mean flow thickness or smaller. As it was shown, the contribution of such waves into the wave spectrum grows with $Fr_\perp$.

First, to verify the present approach of evaluating Pr_t, the analysis was performed on subcritical flow data. The parameter A was found to be 37.9. This is rather close to the value based on other experimental data [2] in an earlier paper [19] ($A = 37.0$). The discrepancy is insignificant and can be explained by different experimental conditions and the absence of measurements in the immediate vicinity of the free surface in [2]. The evaluation of Pr_t in a supercritical flow was then performed using the same approach across the range of the flow parameters that guarantee the K–ε model applicability, i.e. $\alpha \leqslant 50°$ or $Fr_\perp < 700$. Typical examples of matching the experimental data with the calculations by adjusting the parameter A are shown in Fig. 11. Finally, the following approximations have been obtained:

$$A = \begin{cases} 33\text{–}38 & Fr_\perp = 0\text{–}100, \\ 27\text{–}33 & Fr_\perp = 100\text{–}700. \end{cases} \tag{7}$$

In (7), smaller A corresponds to higher $Fr_\perp$. Linear distribution should be used within each sub-range. The evaluated distributions of Pr_t based on a simultaneous use of formulas (6) and (7) along with the previous evaluations for subcritical flows are shown in Fig. 12. These distributions were then used to calculate the Nusselt number in a hydrodynamically fully developed flow with a uniform heat flux applied to the free surface (Fig. 13). To emphasize the effect of the surface waves and turbulence, the same value of Re was used in all calculations, and the Prandtl number was kept high, $Pr = 34$, corresponding to the thermo-physical properties of the molten salts. The Nusselt number was defined as

$$Nu = \frac{qh_m}{k(T_s - T_b)},$$

where T_s and T_b are the mean surface and bulk temperatures, respectively. One can see that the fully developed Nusselt number approximately doubles in the flow with high waviness, in comparison with the same flow with no waves. Also, the increase of $Fr_\perp$ leads to a shorter transition length over which Nu drops to its fully developed magnitude.

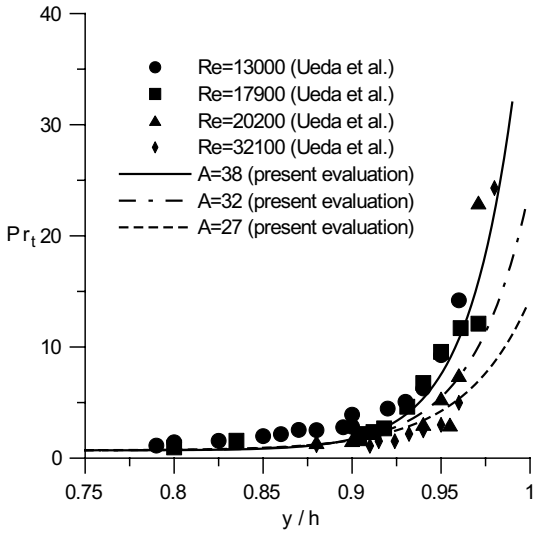

Fig. 12. Turbulent Prandtl number distribution near the free surface for different wavy flows. The symbols correspond to the direct evaluations from [19] based on Ueda's data [2].

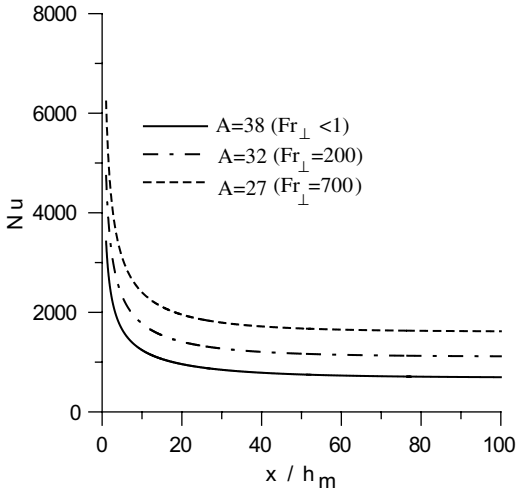

Fig. 13. Local Nusselt number distribution calculated for different wavy flows at $Re = 30{,}000$, $Pr = 34$.

7. Concluding remarks

A key role of $Fr_\perp$ has been revealed. A qualitative description of the processes at a free surface in open channel water flows considered in the present study can be summarized as follows. As $Fr_\perp$ grows, both the free surface and heat transfer rate experience significant changes. An increase in $Fr_\perp$ as the inclination angle grows results in a reduction of the stabilizing effect of gravity against the disturbing effect of turbulence. More and more turbulent structures from the flow bulk reach and disturb the free surface. These disturbances, along with the inherent surface instability, lead to complex wave-type phenomena with both capillary and gravity waves existing at the surface. The gravity waves carry a significant flow rate through the near-surface area, while the capillary-type waves (with wavelengths comparable to the flow thickness and shorter) are mostly responsible for the changes in interfacial heat transport. The effect of $Fr_\perp$ on the wave amplitude in the range of flow parameters stated in Table 1 is approximated very well by Eq. (1). The effect on spectral characteristics lies in shifting towards shorter disturbances as $Fr_\perp$ grows. Both these effects result in better heat transfer conditions through mitigating the blockage effect in the near-surface region.

Comparisons of the standard K–ε model calculations with experimental data show its limitations. The standard model does not properly include a mechanism for turbulence-free surface interaction. That is why it fails to adequately predict the mean flow thickness, if the surface waviness is sufficiently high. The range of applicability of the standard model can also be characterized with $Fr_\perp$. If $Fr_\perp < 2000$, the predictions are within 10% accuracy of the experimental data. At higher $Fr_\perp$, the model predictions are unsatisfactory. In terms of the average wave amplitude, the range of applicability of the model varies widely from subcritical flows, with no waves to those supercritical with the waviness parameter of 0.3.

The near-surface turbulent Prandtl number distributions have been evaluated as a function of $Fr_\perp$ for $Fr_\perp < 700$. These distributions are given by Eqs. (6) and (7). The distribution obtained for Pr_t for a subcritical flow agrees well with the independent evaluations based on the experimental data in [2]. By using these distributions, about a two-time increase in the fully developed Nusselt number for the flow with $Fr_\perp = 700$ has been calculated, in comparison to analogous subcritical flow.

The present study is a part of the ongoing work initiated in [19] by Smolentsev et al. on turbulent open channel flows and heat transfer under fusion reactor conditions. The results currently obtained have showed a need for further improvements of the standard K–ε model as a tool for calculating open surface flows with high waviness. However, a revision of the standard model was beyond the purpose of the paper. The issues of improvements of the calculations are planned to be a principal topic of next work. The ways of extending the model performance can be shortly described as follows. First, the free surface boundary conditions implemented in the present model should be replaced with different conditions more suitable for high waviness flows. Promising boundary conditions for breaking water waves suited for using them with K–ε models have been recently developed in [23]. Second, extra terms in the form of an additional pressure gradient that stands for dynamical effects due to vertical accelerations should be implemented in the momentum equation. Some extra terms in the equation for K will be needed to take into account the effects of energy exchange between the turbulent motion in the flow bulk and the wave modes at the free surface. Third, in situations, when the surface disturbances penetrate all the way down to the bottom wall of the flow, the classic models for the turbulent boundary layer are most likely not applicable any longer. This may require a modification of the low-Reynolds number model presently adopted. All these changes will require a sufficient amount of experimental and theoretical work including efforts on development of turbulence closures and readjustment of the model coefficients.

Acknowledgements

The authors would like to acknowledge the support of the APEX project through DOE Grant DE-FG03-86ER52123 and express their gratitude to Prof. T. Kunugi from Kyoto University, Japan and Prof. S.

Banerjee and his group from UCSB for their valuable comments and discussions.

References

[1] M.A. Abdou et al., Exploring novel high power density concepts for attractive fusion systems, Fusion Eng. Design 45 (1999) 145–167.
[2] H. Ueda, R. Moller, S. Komori, T. Mizushina, Eddy diffusivity near the free surface of open channel flow, Int. J. Heat Mass Transfer 20 (1977) 1127–1136.
[3] S. Komori, H. Ueda, F. Ogino, T. Mizushima, Turbulence structure and transport mechanism at the free surface in an open channel flow, Int. J. Heat Mass Transfer 25 (1982) 513–521.
[4] S. Komori, Turbulence structure and CO_2 transfer at the air–sea interface and turbulent diffusion in thermally stratified flows, CGER Supercomputer Monograph Report, vol. 1, 1996.
[5] S. Kutateladze, Semi-empirical theory of film condensation of pure vapors, Int. J. Heat Mass Transfer 25 (1982) 653–660.
[6] D.P. Frisk, E.J. Davis, The enhancement of heat transfer by waves in stratified gas-liquid flow, Int. J. Heat Mass Transfer 15 (1972) 1537–1552.
[7] V.E. Nakoryakov, B.G. Pokusaev, K.B. Radev, Waves and their effect on convective gas diffusion in falling liquid films, in Russian, Zhurn. Prikl. Mekh. Tekh. Fiz. 3 (1987) 95–104.
[8] J.T. Davies, Turbulence Phenomena, Academic, 1972.
[9] M. Brocchini, D.H. Peregrine, The dynamics of strong turbulence at free surfaces. Part 1. Description, J. Fluid Mech. 449 (2001) 225–254.
[10] B.Freeze, Ph.D. Dissertation, UCLA, 2002.
[11] S. Smolentsev, B. Freeze, N. Morley, M. Abdou, Experimental study of turbulent supercritical open channel water flow as applied to the CLiFF concept, Fusion Eng. Des. 63–64 (2002) 397–403.
[12] A.S. Telles, A.E. Dukler, Statistical characteristics of thin, vertical, wavy, liquid films, Ind. Eng. Chem. Fundam. 9 (1970) 412–421.
[13] K.J. Chu, A.E. Dukler, Statistical characteristics of thin, wavy films: Part II. Studies of the substrate and its wave structure, AIChE J. 20 (1974) 695–706.
[14] K.J. Chu, A.E. Dukler, Statistical characteristics of thin, wavy films: Part III. Structure of the large waves and their resistance to gas flow, AIChE J. 21 (1975) 583–593.
[15] L.S.Cohen, Ph.D. Dissertation, University of Illinois, 1964.
[16] S.K. Mitra, J.F. Kaiser (Eds.), Handbook for Digital Signal Processing, John Willey & Sons, 1993.
[17] K.Y. Chien, Predictions of channel and boundary layer flows with a low-Reynolds number turbulence model, AIAA J. 20 (1982) 33–38.
[18] W.Rodi, Turbulence models and their application in hydraulics: a state of the art review, International Association for Hydraulic Research, Delft, the Netherlands, 1984.
[19] S. Smolentsev, M. Abdou, N. Morley, A. Ying, T. Kunugi, Application of the K-epsilon model to open channel flows in a magnetic field, Int. J. Eng. Sci. 40 (2002) 693–711.
[20] F.G. Blottner, Variable grid scheme applied to turbulent boundary layers, Comput. Meth. Appl. Mech. Eng. 4 (1974) 179–194.
[21] B.D. Nichols, C.W. Hirt, Calculating three-dimensional free surface flows in the vicinity of submerged and exposed structures, J. Comp. Phys. 12 (1973) 234–246.
[22] I. Nezu, H. Nakagawa, Turbulence in open-channel flows, IAHR AIRH Monograph Series, 1993.
[23] M. Brocchini, Free surface boundary conditions at a bubbly/weakly splashing air-water interface, Phys. Fluids 14 (2002) 1834–1840.